Ultralow-Threshold and High-Quality Whispering-Gallery-Mode Lasing from Hybrid-shell Colloidal Quantum Wells

Rui Duan[#], Zitong Zhang[#], Lian Xiao, Xiaoxu Zhao, Yi Tian Thung, Lu Ding, Zheng Liu, Jun Yang, Van Duong Ta*, Handong Sun**

R. Duan, Z. T. Zhang, Dr. L. Xiao, Y. T. Thung, Dr. V. D. Ta, Prof. H. D. Sun
Division of Physics and Applied Physics, School of Physical and Mathematical Sciences, Nanyang Technological University, 637371, Singapore

Dr. X. X. Zhao, Prof. Z. Liu
School of Materials Science and Engineering, Nanyang Technological University, 639798, Singapore

Prof. Z. Liu
School of Electrical and Electronic Engineering, Nanyang Technological University, 639798, Singapore
CINTRA CNRS/NTU/THALES, UMI 3288, 637553, Singapore

Dr. L. Ding
Institute of Materials Research and Engineering, A*STAR (Agency for Science, Technology and Research), Singapore 138634, Singapore

R. Duan
College of Physics and Optoelectronic Engineering, Harbin Engineering University, Harbin 150001, China

Prof. J. Yang
Guangdong Provincial Key Laboratory of Information Photonics Technology, College of Information Engineering, Guangdong University of Technology, Guangzhou 510006, China

Dr. V. D. Ta
Department of Optical Devices, Le Quy Don Technical University, Hanoi 100000, Vietnam

[#] R. Duan and Z. T. Zhang contributed equally to this work.
* E-mail: yangj@gdut.edu.cn; duong.ta@lqdtu.edu.vn; HDSun@ntu.edu.sg

Keywords: colloidal quantum wells, compositional engineering, whispering gallery modes, single-mode lasing, ultralow threshold lasing, monolithic microcavity

Abstract: The realization of efficient on-chip microlasers with scalable fabrication, ultralow threshold, and stable single-frequency operation is always preferred for a wide range of miniaturized photonic systems. Herein, an effective way to fabricate nanostructures-whispering-gallery-mode (WGM) lasers by simply drop-casting CdSe/CdS@$Cd_{1-x}Zn_xS$ core/buffer-shell@graded-shell nanoplatelets (NPLs) solution onto silica microspheres has been presented. Thanks to the excellent gain properties from the interface engineered core/shell NPLs and high-quality factor inherent from the WGM resonator, the proposed microsphere lasers show a record-low lasing threshold of 3.26 μJ cm^{-2} among all NPLs-based lasing demonstrations under ns laser pumping. The presence of sharp discrete transverse electric- and magnetic-mode spikes, the inversely proportional dependence of the free spectra range on the size of microsphere and the polarization anisotropy of laser output represent the direct experimental evidence for NPLs-WGM lasing nature, which is verified theoretically by the computed electric-field distribution inside the microcavity. Remarkably, a stable single-mode lasing output with an ultra-low lasing threshold of 3.84 μJ cm^{-2} is achieved by the Vernier effect through evanescent field coupling. Our results highlight the significance of interface engineering on the optimization of gain properties of heterostructured nanomaterials and shed light on developing future miniaturized tunable coherent light sources.

1. Introduction

Miniaturized lasers have attracted much attention in the fields of nanoscale optical integration,[1-3] coherent sensing,[4-7] and optical information processing.[8,9] As such, a broad range of solution-processable materials, such as organic dye molecules and colloidal semiconductor nanostructures, with low-cost production and easy incorporation into various cavities, have been the core gain media of intense research for lasing demonstration. [1,7,10-13] Among all these solution-processable gain materials, two-dimensional (2-D) colloidal nanoplatelets (NPLs) with pure quantum confinement from the vertical direction,[14,15] also defined as semiconductor quantum wells, have become the most promising alternative owing to the suppressed non-radiative Auger recombination (AR) rates relative to their 0-D quantum dots and 1-D nanorods counterparts and their long-term stable lasing performance compared to traditional organic dyes suffering from severe irreversible photobleaching.[12,16] In addition, thanks to the persistent efforts made by researchers, various approaches including thickness tunability, ligand exchange, and heterostructure-engineering have been reported to manipulate the excitonic characteristics of the final NPLs products with emission covering the whole visible spectral regime.[17] Rapid AR process competing against the population inversion is the main loss channel of the lasing action for the low-dimensional gain medium. Very recently, CdSe core NPLs sandwiched between compositionally graded $Cd_{1-x}Zn_xS$ shells have exhibited an unprecedented ultralow threshold of 3 μJ cm^{-2} for the onset of amplified spontaneous emission (ASE) owing to their slowed AR process resulting from the smoothening of the interface potential barrier and the perfect surface passivation.[18,19] Driven by their remarkable gain properties, numerous works have been conducted on the demonstration of core/alloying shell NPLs-based lasers.[20-24]

To date, the majority of works using NPLs as a gain medium have adopted several optical feedback configurations including Fabry−Pérot cavity,[10,11,19,20,22,25-27] photonic-crystal cavity,[23,28] random cavity as well as distributed feedback cavity.[21,29] However, NPLs-whispering gallery mode (WGM) lasers with ultra-high quality (Q) factor and extremely small mode volume, [30,31] in which the closed feedback loop is formed via total internal reflection in the boundaries of high refractive index cavity, are rarely studied. WGM resonant cavities, which can greatly enhance the interaction between light and matter, have already demonstrated remarkable applications in such as ultra-high-sensitivity sensing,[4,5,32,33] integrated optics,[34-36] quantum optics,[37,38] and nonlinear optics.[39,40] Although coreless fiber-assisted NPLs-WGM laser has been demonstrated previously, only multi-mode lasing action with prominent spontaneous emission background and high lasing threshold up to hundreds of μJ cm^{-2} under

femtosecond pulsed-laser pump wwa presented,[24] which hinders the practical utilization. In addition, the dipping preparation method used in this work usually requires to precisely control the movement of fibers at slow speed in concentrated dispersion to ensure the smoothness and uniformity of the coated closed-packed film formed via the adhesion process.[41] Consequently, successful demonstration of NPLs-WGM resonators with scalable simple production and ultralow lasing threshold is urgently demanded in the field of miniaturized solid-state lasers.

Herein, NPLs-WGM microlasers with tunable longitudinal modes and easy preparation method are developed by directly drop-casting newly-engineered CdSe/CdS@$Cd_{1-x}Zn_xS$ core/buffer-shell@graded-shell NPLs dispersion onto silica microspheres with different sizes. The outstanding gain features of as-synthesized core/shell NPLs are characterized in detail and attributed to the release of interface strain by the introduction of CdS buffer layer together with the reduced AR rates and strong quantum confinement effects owing to the inclusion of alloying $Cd_{1-x}Zn_xS$ outer shell with type-I band alignment. These unique NPLs-WGM microsphere lasers exhibit a record low lasing threshold down to 3.26 μJ cm^{-2} and reliable lasing stability (9% decrease of lasing intensity) under continuous high pumping excitations for 100 minutes. Furthermore, the WGM mechanism is systematically verified by experimental results including detailed mode analysis, size-dependent free spectra range, and high polarization factor of lasing outputs up to 0.79 as well as simulated electric-field profile inside microsphere resonators. Remarkably, with the help of the Vernier effect, high-quality and stable single-mode lasing with ultralow threshold of 3.84 μJ cm^{-2} is successfully achieved.

2. Results and Discussion

2.1. Characterization of Engineered CdSe/CdS@$Cd_{1-x}Zn_xS$ Core/Shell NPLs

Our colloidal CdSe/CdS@$Cd_{1-x}Zn_xS$ Core/Shell NPL consists of an atomically-flat CdSe NPLs with 1.2 nm thickness as a core which is sandwiched between the inner CdS buffer-shell and the outer $Cd_{1-x}Zn_xS$ graded shell. In principle, this specifically-engineered hybrid-shell structure takes three roles. Firstly, introduction of CdS buffer shell significantly reduces interface defects caused by the large lattice mismatch between CdSe core and outer $Cd_{1-x}Zn_xS$ shell.[42,43] Secondly, graded $Cd_{1-x}Zn_xS$ shell with smooth interface potential transition suppresses the AR rates which is large in core/shell NPLs with sharp interface potential transition due to rigid momentum conservation.[44,45] Last but not least, CdSe/$Cd_{1-x}Zn_xS$ has type-I band alignment and provides strong spatial confinement on the photoexcited electron-hole pairs which leads to superior gain features and inhibits the interaction between excitons and surface defects, whereas CdSe/CdS forms type-II band alignment where electron-hole pairs

are delocalized over the whole system.[18,19,46] **Figure 1**a presents the absorption spectrum with well-resolved heavy- and light-hole excitonic transitions and photoluminescence (PL) spectrum with narrow full width at half maximum (FWHM) down to 18 nm. High resolution HAADF-STEM (High-angle annular dark-field scanning transmission electron microscopy) image shown in **Figure 1**b also proves the uniform rectangular shape of as-prepared NPLs without noticeable etched edges. Moreover, the clear contrast between bright core and dark shell sections owing to their different composition is recognized in **Figure 1**c.

To evaluate the gain properties of these core/shell NPLs, ASE measurements using stripe excitation geometry under femtosecond laser pumping were conducted (see the Supporting Information Add section number). As shown in **Figure S1**, a narrower emission band emerges on the red side of the spontaneous emission band as the pump fluence keeps increasing, which indicates the appearance of stimulated emission (or ASE) and signifies the existence of multiexcitonic gain mechanism for the NPLs.[10,18,25-27] The dependence of integrated emission intensity on pump fluence in **Figure 1**d indicates the ASE threshold of $P_{th} \sim 4$ μJ cm^{-2}, which is comparable to the previously reported state-of-the-art core/shell NPLs.[18,19] Variable stripe length (VSL) measurements were also performed to derive the modal gain coefficient *G* of the NPL thin film (see the Supporting Information Add section number). The pump fluence was fixed at $2P_{th}$, for a clear comparison of the gain behaviors with the previously reported CdSe/CdS@$Cd_{1-x}Zn_xS$ core/crown@shell NPLs.[24] As shown in **Figure 1**e, the calculated *G* of 202 cm^{-1} from our NPLs outperforms the previously reported NPLs with core/crown@shell structures,[24] which further validates the significant effects of the proposed hybrid shell on the modification of the corresponding efficient gain.

2.2. Fabrication and Characterization of NPLs-based Microsphere Laser

Figure 2a illustrates the schematic of a NPLs-coated SiO_2 microsphere that supports WGMs with the emitted light propagating in the high refractive index NPLs spherical shell via total internal reflection (see the Supporting Information Add section number). Scanning electron microscopy (SEM) images of the individual SiO_2 microsphere before and after drop-coating with NPLs as well as the cluster consisting of several NPLs-coated microspheres with different sizes in the range between 10 μm to 120 μm are displayed in **Figures 2**b-d. NPLs are conformally coated on the microspheres which preserve the perfect spherical shape and have smooth surface. More SEM images and optical microscope photographs of microspheres with various diameter are shown in **Figures S2** and **S3**. **Figures 2**e-f are the cross-section profile of a NPLs shell cracker peeled off from SiO_2 microspheres. The thickness of the NPLs gain layer is about 490 nm. Energy dispersive spectrometer (EDS) mapping reveals the uniform coverage

of NPLs on the microsphere as shown in **Figures 2**g-k and **Figure S4**. The smooth morphology and uniform distribution of NPLs gain medium on the microsphere's surface effectively alleviate the scattering loss for optical resonance and eventually lead to the low-threshold laser operation which will be discussed below.

2.3. WGM Lasing

2.3.1. Multi-mode Lasing

NPLs-WGM microlasers were characterized by a home-built micro-photoluminescence (μ-PL) system using 532 nm nanosecond pulsed laser excitation (1 ns, rep. rate 60Hz) (see **Figure S5** and Experimental Section). The lasing operation of individual NPLs-WGM microlasers of various sizes is demonstrated by the spectral analysis shown in **Figure 3**. For a microsphere with diameter of 12 μm (**Figure 3**a), broad spontaneous emission is peaked at ~655 nm under low pump fluence. With the increase of pump fluence, sharp lasing spikes with regular intervals and the rapidly boosted PL intensity are clearly observed. **Figure 3**b plots the integrated PL intensity and FWHM of emission peaks as a function of the pump fluence. Clear threshold behavior confirms the lasing action from the microlasers. Compared with the previously reported lasing features of NPLs-based lasers listed in **Table 1**, our NPLs-WGM microspheres exhibit the record-low threshold of 3.26 μJ cm^{-2} and high *Q*-factor up to ~ 4200 (see analysis in **Figure S6**), which is mainly due to the excellent gain material and ultralow loss optical cavity with small surface roughness. Good refractive index contrast between NPLs and air or SiO_2 as well as suitable NPLs thickness ensure excellent confinement of both pump and emitted light in NPLs layer for generating lasing oscillations. It is noteworthy that the lowest lasing threshold is generated from the NPLs-WGM microsphere with a moderate diameter (~20 μm), which is attributed to the trade-off between the stronger light confinement and accelerated surface scattering as increasing the diameter of the spherical NPLs-WGM cavity.

The WGM lasing mechanism is further confirmed by analyzing the spectral characteristics of these microsphere lasers. In general, WGM lasing peaks, characterized by transverse magnetic (TM) or transverse electric (TE) modes, could be well examined from the asymptotic equation (see Supplementary Information add section number). **Figure 4**a displays the typical output spectrum of a 20 μm-diameter NPLs-WGM microsphere. The good agreement of the positions of laser modes between the experimental measurement and the fitting results further confirms the WGM lasing mechanism in our NPLs-coated microsphere. According to our theoretical calculation, the lasing peaks pertain to first order (q =1) and the longitudinal mode numbers count from 163 to 166 for the TE and TM modes, respectively. Another typical characteristic of WGM lasing is the size-dependent free spectral range (*FSR*). For spherical

WGM resonator used in our case, *FSR* could be calculated as follow:[7,47]

$$FSR=\lambda^2/(n_{eff}\pi D) \quad (1)$$

where λ, n_{eff} and D represent the peak wavelength, effective refractive index and the diameter of NPLs-WGM microcavity, respectively. **Figure 4**b plots a series of lasing spectra collected from the microsphere with different sizes. The inverse proportional dependence of *FSR* on *D* (in **Figure 4**c and **Figure S7)** unambiguously disclosed the WGM nature of our fabricated microlaser. Pointedly, the derived effective refractive index n_{eff} in Equation (1) is 1.76, which is smaller than that of pure NPLs film extracted from ellipsometry measurements as shown in **Figure S8**. The smaller n_{eff} is tentatively attributed to a tiny fraction of the WGM electric field leaking into the surrounding air environment and the adjacent silica sphere, which is also consistent with the simulated electric field profile elaborated below. The finite element method provided by COMSOL Multiphysics was used to numerically simulate the electric field distribution in the NPLs-coated microsphere laser (see details of the simulation model and **Figure S9** in Supplementary Information). All simulation parameters are consistent with the actual measured parameters. The effective refractive index of the microcavity n_{seff} employed in the simulation model is 1.74, which is close to the calculated n_{eff} = 1.76 from Equation (1). **Figures 4**d-g present the cross-sectional view of the electric field distribution inside the resonant cavity. As expected, the light produced a strong WGM resonance and is effectively confined in the gain layer through the total internal reflection with only a few leaking into the adjacent domain of the microcavity. Upon close examination of the normalized electric field intensity in the radial direction shown in **Figure S10**, only 3.87% and 1.42% of the waves leak into the air and SiO_2 layer, respectively. This small fraction of field leakage through evanescent waves is another evidence for the proposed spherical microlaser to support lasing operation with such high *Q*-factor and low threshold.

Microlasers with linear polarization and reliable photostability have extensive practical applications in signal detection, fundamental research, and display technology. To study the polarization anisotropy of the NPL-WGM microlaser, the laser emission spectra as a function of rotation angle (θ) with respect to a linear polarizer below and above lasing threshold were recorded for comparison. From **Figures 5**a-b, little change in the PL intensity is observed with the variation of θ, indicating a very low polarization ratio below the threshold. However, the lasing action above the threshold presented in **Figures 5**c-d is strongly polarized with the dominant optical feedback path perpendicular to the equatorial plane, which is also observed in other spherical WGM-assisted lasers from previous studies.[48-50] This polarization anisotropy is consistent with the feature of WGM lasing. The polarization anisotropy could be

quantitatively reflected from the factor of the polarization state defined as[51]

$$R = \frac{I_{max} - I_{min}}{I_{max} + I_{min}} \quad (2)$$

where I_{max} and I_{min} correspond to the maximum and minimum lasing emission intensity, respectively. R of our proposed NPLs-WGM laser is determined to be 0.79, which is higher than that from the previously proposed NPLs-embedded fiber laser.[17] Environmental degradation and thermal stability are two insurmountable barriers limiting the lasing durability of nanostructures-based microlasers. **Figure 5**e illustrates the evolution of the lasing intensity of a NPLs-WGM laser under continuous and strong nanosecond pulse excitation for 100 minutes at in ambient conditions. It should be mentioned that the pumped excitation was already one order of magnitude larger than the lasing threshold. The results show that all lasing peaks are kept at the same position and no significant quenching of lasing output (less than 9% decrease of intensity) or chemical degradation is observed during the measurement. The excellent photostability and resistance to the harsh environment afforded by NPLs-WGM microlaser provide further evidence that our choice of gain material and microsphere cavity offer the guidelines for fabricating a robust, high-performance miniature laser application.

2.3.2. Single-mode Lasing

Although single-mode lasers are highly desirable in the fields of optical communications, optical storage, and optical sensing, the achievement of single-frequency WGM-lasing operation is difficult as the cavity is expected to support only one mode over the entire gain spectrum range.[52-54] Thus, the conventional strategy to realize single-mode WGM operation is to expand the *FSR* by reducing the size of the optical cavity until there is only one mode in the whole gain range according to **Equation 1**.[7] Unfortunately, the reduction of cavity size will inevitably deteriorate the *Q*-factor and result in the attenuation of the lasing output with high optical loss. The alternative approach is to exploit the Vernier effect in which the shared resonance mode of the individual cavities will be enhanced while the other modes will be suppressed in coupled microspheres.[55,56] Here, we try to validate the feasibility of attaining single-mode lasing operation through the Vernier effect from two strongly coupled NPLs-coated microspheres as depicted in **Figure 6**a. **Figure 6**b presents the lasing spectra of each isolated NPLs-WGM microsphere at a pump fluence of 14.79 μJ cm^{-2}, and the diameters of these two microspheresare 48 μm (D_1) and 44 μm (D_2), respectively. *FSR* of the coupled microspheres can be estimated by Vernier equation ($D_1 > D_2$),[57,58]

$$FSR = \lambda^2 / [\pi n_{eff} (D_1 - D_2)] \quad (3)$$

Considering that the resonance wavelength is about 663.28 nm, the theoretically calculated

FSR is 19.9 nm, which has already exceeded the gain spectral range, even the PL spectral width of as-synthesized NPLs. **Figure 6**c plots the results of single-mode lasing emission from this strong coupling system under different pump intensities, which reveals that the excitation power for the onset of the stable single-mode lasing performance is only about 3.84 μJ cm^{-2}, much smaller than that of NPLs-WGM microsphere with reduced size according to **Figure 3**. Our achievement shows that by integrating two isolated NPLs-WGM microspheres into the coupled system, the single-frequency operation with record-low lasing threshold via the Vernier effect is achieved for the first time in the field of laser demonstrations containing colloidal quantum-well semiconductor materials.

3. Conclusion

In summary, thanks to the choice of interface-engineered core/shell NPLs with remarkable gain properties and appropriate spherical microcavity with high *Q*-factor, an ultralow-threshold multimode and single-mode NPLs-WGM laser is proposed and demonstrated by simply drop-casting high-concentrated dispersion onto silica microsphere cavity. Based on the comprehensive spectroscopic analysis, typical WGM-lasing characteristics such as diameter- and polarization-dependent lasing features as well as excellent photostability are unambiguously revealed for the first time in the field of NPLs-WGM laser, showing a good agreement with the numerical calculation of the electromagnetic field profile for quantitative comparison. Besides, the single-frequency operation with a record-low lasing threshold of 3.84 μJ cm^{-2} is demonstrated from strongly-coupled microspheres system via the Vernier effect. Our work offers a compact, robust, and universal fabrication method towards fascinating colloidal nanomaterials-based high-quality single-mode coherent light source covering the visible spectral region.

Supporting Information

Supporting Information is available from the Wiley Online Library or from the author.

Acknowledgements

R. Duan and Z. T. Zhang contributed equally to this work. This work is supported by NRF-CRP21-2018-0007, NRF-CRP23-2019-0007 and AME-IRG- A20E5c0083. The electron microscopy imaging was performed at the Facility for Analysis, Characterization, Testing, and Simulation (FACTS) at Nanyang Technological University, Singapore. J. Y. also acknowledges the support from the National Science Fund for Distinguished Young Scholars of China

(61925501), the Guangdong Introducing Innovative and Enterpreneurial Teams (2019ZT08X340) and Introducing Leading Talents (2019CX01X010) of "The Pearl River Talent Recruitment Program" of Guangdong Province.

Received: ((will be filled in by the editorial staff))
Revised: ((will be filled in by the editorial staff))
Published online: ((will be filled in by the editorial staff))

Reference

[1] Y.-S. Park, J. Roh, B. T. Diroll, R. D. Schaller, V. I. Klimov, *Nat. Rev. Mater*. **2021**, *6*, 382.

[2] G.-Q. Wei, X.-D. Wang, L.-S. Liao, *Laser Photonics Rev.* **2020**, *14*, 2000257.

[3] L. Yang, L. Li, Q. Wang, C. Xing, L. Ma, Y. Zeng, Y. Zhao, Y. Yan, *Adv. Optical Mater.* **2019**, *7*,1901228.

[4] N. Toropov, G. Cabello, M. P. Serrano, R. R. Gutha, M. Rafti, F. Vollmer, *Light Sci. Appl.* **2021**, 10, 42.

[5] X. F. Jiang, A. J. Oavi, S. H. Huang L. Yang, *Matter* **2020**, *3*, 371.

[6] R. Duan, Y. Li, H. Li, J. Yang, *Biomed. Opt. Express* **2019**, *10*, 6073.

[7] V. D. Ta, R. Chen, L. Ma, Y. J. Ying, H. D. Sun, *Laser Photonics Rev.* **2013**, *7*, 133.

[8] Z. Z. Liu, S. H. Huang, J. Du, C. W. Wang, Y. X. Leng, *Nanophotonics **2020**, 9*, 2251.

[9] A. E. Zhukov, N. V. Kryzhanovskaya, E. I. Moiseev, M. V. Maximov, *Light: Sci. Appl.* **2021**, *10*, 80.

[10] J. Q. Grim, S. Christodoulou, F. D. Stasio, R. Krahne, R. Cingolani, L. Manna, I. Moreels, *Nat. Nanotechnol.* **2014**, *9*, 891.

[11] J. Yu, M. Sharma, M. Li, S. Delikanli, A. Sharma, M. Taimoor, Y. Altintas, J. R. McBride, T. Kusserow, T. C. Sum, H. V. Demir, C. Dang, *Laser Photonics Rev*. **2021**, *15*, 2100034.

[12] J. Yu, C. Dang, *Cell Rep. Phys. Sci*. **2021**, *2*, 100308.

[13] Y. Wang, K. E. Fong, S. Yang, V. D. Ta, Y. Gao, Z. Wang, V. Nalla, H. V. Demir, H. Sun, *Laser Photonics Rev.* **2015**, *9*, 507.

[14] Z. T. Zhang, Y. T. Thung, X. Chen, L. Wang, W. Fan, L. Ding, H. D. Sun, *J. Phys. Chem. Lett.* **2021**, *12*, 191.

[15] Z. T. Zhang, H. D. Sun, *Adv. Photonics Res.* **2021**, *2*, 2100045.

[16] C. E. Rowland, I. Fedin, H. Zhang, S. K. Gray, A. O. Govorov, D. V. Talapin, R. D. Schaller, *Nat. Mater.* **2015**, *14*, 484.

[17] Z. T. Zhang, Y. T. Thung, L. Wang, X. Chen, L. Ding, W. Fan, H. D. Sun, *J. Phys. Chem. Lett.* **2021**, *12*, 9086.

[18] Y. Kelestemur, Y. Shynkarenko, M. Anni, S. Yakunin, M. L. De Giorgi, M. V. Kovalenko, *ACS Nano* **2019**, *13*, 13899.

[19] Y. Altintas, K. Gungor, Y. Gao, M. Sak, U. Quliyeva, G. Bappi, E. Mutlugun, E. H. Sargent, H. V. Demir, *ACS Nano* **2019**, *13*, 10662.

[20] J. Maskoun, N. Gheshlaghi, F. Isik, S. Delikanli, O. Erdem, E. Y. Erdem, H. V. Demir, *Adv. Mater.* **2021**, *33*, e2007131.

[21] N. Gheshlaghi, S. Foroutan-Barenji, O. Erdem, Y. Altintas, F. Shabani, M. H. Humayun, H. V. Demir, *Nano Lett.* **2021**, *21*, 4598.

[22] S. Foroutan-Barenji, O. Erdem, S. Delikanli, H. B. Yagci, N. Gheshlaghi, Y. Altintas, H. V. Demir, *Laser Photonics Rev.* **2021**, *15*, 2170024.

[23] M. Wu, S. T. Ha, S. Shendre, E. G. Durmusoglu, W. K. Koh, D. R. Abujetas, J. A. Sanchez-Gil, R. Paniagua-Dominguez, H. V. Demir, A. I. Kuznetsov, *Nano Lett.* **2020**, *20*, 6005.

[24] M. Sak, N. Taghipour, S. Delikanli, S. Shendre, I. Tanriover, S. Foroutan, Y. Gao, J. Yu, Z. Yanyan, S. Yoo, C. Dang, H. V. Demir, *Adv. Funct. Mater.* **2020**, *30*, 1907417.

[25] C. She, I. Fedin, D. S. Dolzhnikov, P. D. Dahlberg, G. S. Engel, R. D. Schaller, D. V. Talapin, *ACS Nano* **2015**, *9*, 9475.

[26] M. Li, M. Zhi, H. Zhu, W. Y. Wu, Q. H. Xu, M. H. Jhon, Y. Chan, *Nat. Commun.* **2015**, *6*, 8513.

[27] B. Guzelturk, Y. Kelestemur, M. Olutas, S. Delikanli, H. V. Demir, *ACS Nano* **2014**, *8*, 6599.

[28] Z. Yang, M. Pelton, I. Fedin, D. V. Talapin, E. Waks, *Nat. Commun.* **2017**, *8*, 143.

[29] Y. Gao, M. Li, S. Delikanli, H. Zheng, B. Liu, C. Dang, T. C. Sum, H. V. Demir, *Nanoscale* **2018**, *10*, 9466.

[30] G. C. Righini, Y. Dumeige, P. Féron, M.Ferrari, G. N. Conti, D. Ristic, S. Soria, *Riv. Nuovo Cim* **2011**, *34*, 435.

[31] K. J. Vahala, *Nature* **2003**, *424*, 839.

[32] R. Duan, X. Hao, Y. Li, H. Li, *Sens. Actuators, B* **2020**, *308*, 127672.

[33] T. Reynolds, N. Riesen, A. Meldrum, X. Fan, J. M. M. Hall, T. M. Monro, and A. Francois, *Laser Photonics Rev.* **2017**, *11*, 1600265.

[34] O. Kfir, H. L. Martins, G. Storeck, M. Sivis, T. R. Harvey, T. J. Kippenberg, A. Feist, C.Ropers, *Nature* **2020**, *582*, 46.

[35] Y. Peng, J. Lu, D. Peng, W. Ma, F. Li, Q. Chen, X. Wang, J. Sun, H. Liu, C.Pan, *Adv. Funct. Mater.* **2019**, *29*, 1905051.

[36] J. Feldmann, N. Youngblood, C. D. Wright, H. Bhaskaran, W. H. P. Pernice, *Nature* **2019**, *569*, 208.

[37] A. E. Arumona, I. S. Amiri, S. Punthawanunt, P. Yupapin, *Opt. Quant. Electron.* **2020**, *52*, 208.

[38] Y. Zhou, Z. Chen, J. T. Shen, *Phys. Rev. A* **2020**, *101*, 043831.

[39] Q. Wang, X. F. Jiang, G. M. Zhao, M. Z. Zhang, C. W. Hsu, B. Peng, A. D. Stone, L. Jiang, L. Yang, *Nat. Phys.* **2020**, *16*, 334.

[40] W. Chen, S. K. Özdemir, G. Zhao, J. Wiersig, L. Yang, *Nature* **2017**, 548, 192.

[41] W. Wang, M. Zhang, F. Deng, Z. Wang, Y. Wang, *Appl. Phys. Lett.* **2021**, *119*, 051102.

[42] A. A. Rossinelli, A. Riedinger, P. Marques-Gallego, P. N. Knusel, F. V. Antolinez, D. J. Norris, *Chem Commun.* **2017**, *53*, 9938.

[43] Y. Altintas, U. Quliyeva, K. Gungor, O. Erdem, Y. Kelestemur, E. Mutlugun, M. V. Kovalenko, H. V. Demir, *Small* **2019**, *15*, e1804854.

[44] Y. S. Park, W. K. Bae, L. A. Padilha, J. M. Pietryga, V. I. Klimov, *Nano Lett.* **2014**, *14*, 396.

[45] Y. S. Park, W. K. Bae, T. Baker, J. Lim, V. I. Klimov, *Nano Lett.* **2015**, *15*, 7319.

[46] A. A. Rossinelli, H. Rojo, A. S. Mule, M. Aellen, A. Cocina, E. De Leo, R. Schäublin, D. J. Norris, *Chem. Mater.* **2019**, *31*, 9567.

[47] S. Yang, Y. Wan, H. D. Sun, *Adv. Optical Mater.* **2015**, *3*, 1136–1162

[48] B. Zhou, Y. Zhong, M. Jiang, J. Zhang, H. Dong, L. Chen, H. Wu, W. Xie, L. Zhang, *Nanoscale*, **2020**, *12*, 5805-5811.

[49] X. Fu, X. Fu, Y. Chen, L. Qin, H. Peng, R. Shi, F. Li, Q. Zhou, Y. Wang, Y. Zhou, Y. Ning, *J. Phys. Chem. Lett.* **2020**, *11*, 541-547.

[50] H. Zhang, C. Zhao, S. Chen, J. Tian, J. Yan, G. Weng, X. Hu, J. Tao, Y. Pan, S. Chen, H. Akiyama, J. Chu, *Chem. Eng. J.* 2020, *389*, 124395.

[51] J. Hu, L. S. Li, W. Yang, L. Manna, L. W. Wang, A. P. Alivisatos, *Science* **2001**, *292*, 2060.

[52] L. Feng, Z. Wong, R. M. Ma, Y. Wang, X. Zhang, *Science* **2014**, *346***,** 972.

[53] W. Liu, M. Li, R. S. Guzzon, E. J. Norberg, J. S. Parker, M. Lu, L. A. Coldren, J. Yao, *Nat. Commun.* **2017**, *8*, 15389.

[54] K. Rong, F. Gan, K. Shi, S. Chu, Jianjun Chen, *Adv. Mater.* **2018**, *30*, 1706546.

[55] K. Oda, N. Takato, H. Toba, *J. Lightwave Technol*.**1991**, *9*, 728.

[56] G. Griffel, *IEEE Photonics Technol. Lett.* **2000**, *12*, 1642.

[57] L. Shang, L. Liu, L. Xu, *Opt. Lett.* **2008**, *33*, 1150.

[58] V. D. Ta, R. Chen, and H. Sun, *Adv. Optical Mater.* **2014**, *2*, 220.

[59] R. Sapienza, *Nat. Rev. Phys.* **2019**, *1*, 690.

[60] X. Li, Y. Wang, H. D. Sun, H. Zeng, *Adv. Mater.* **2017**, *29*, 1701185.

[61] F. Luan, B. Gu, A. S. Gomes, K.-T. Yong, S. Wen, P. N. Prasad, *Nano Today* **2015**, *10*, 168.

Table 1. Thresholds and Q-factors of CdSe NPLs-based lasers.

Lasing Type	Gain materials	Threshold	*Q*-factor	References
VCSE Lasing	CdSe/CdS C/C NPLs	2.49 mJ/cm^2	~270	[27]
Random lasing	CdSe/CdSeTe C/C NPL	950 μJ/cm^2	~1700	[25]
Mie resonances lasing	CdSe/$Cd_{1-x}Zn_xS$ C/S NPLs	36 μJ/cm^2	*2590*	[23]
DBR lasing	CdSe/$Cd_{1-x}Zn_xS$ C/S NPLs	23 μJ/cm^2	~1100	[21]
F-P lasing	CdSe/CdS@$Cd_{1-x}Zn_xS$ C/C @shell NPLs	68.4 μJ/cm²	1195	[20]
WGM lasing	CdSe/CdS@$Cd_{1-x}Zn_xS$ C/C@Shell NPLs	188 μJ/cm^2	~480	[24]
WGM lasing	CdSe/CdS@$Cd_{1-x}Zn_xS$ C/S NPLs	3.26 μJ/cm^2	*~4200*	*Our work*

[a] VCSE, Vertical Cavity Surface Emitting; DBR, Distributed Bragg Reflector; F-P, Fabry–Pérot; C/C, Core/Crown; C/S, Core/Shell.

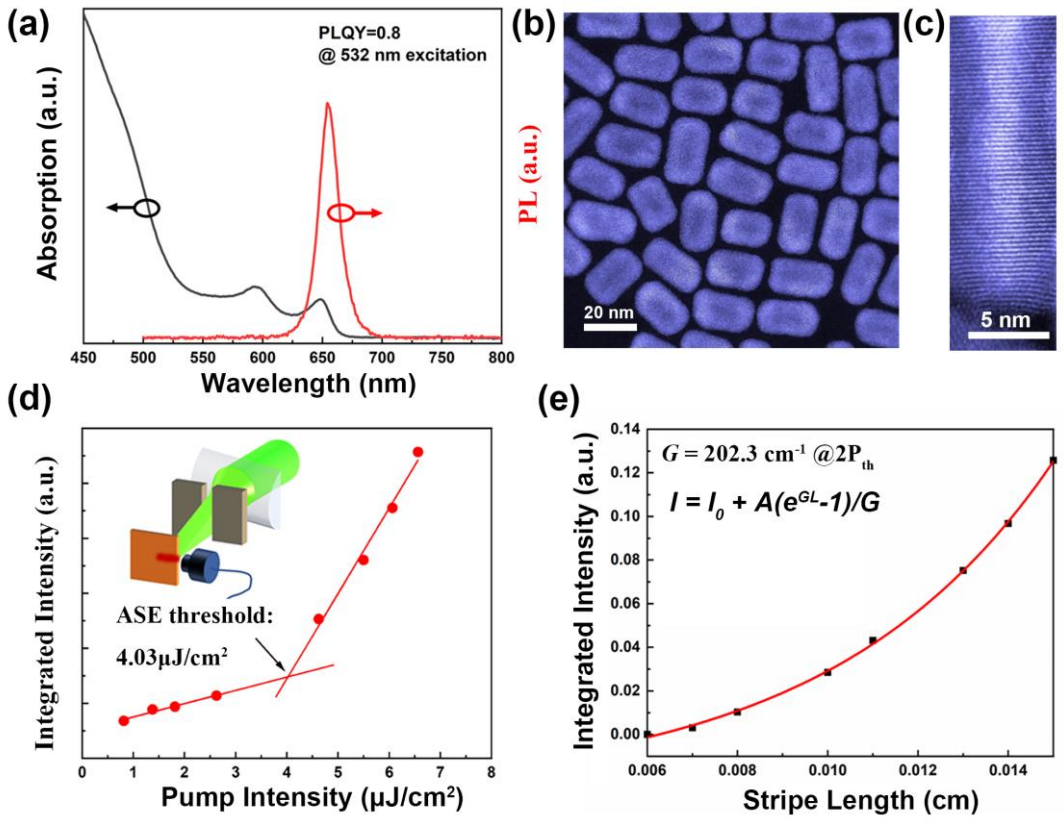

Figure 1. a) PL and absorption spectra of the as-synthesized NPLs. High resolution HAADF STEM images of b) top-view core/shell NPLs and c) side-view a single core/shell NPL. d) The integrated edge emission intensity with the pump intensity. The inset shows the schematic diagram for ASE and gain measurement. e) The integrated PL intensity with the change of stripe length.

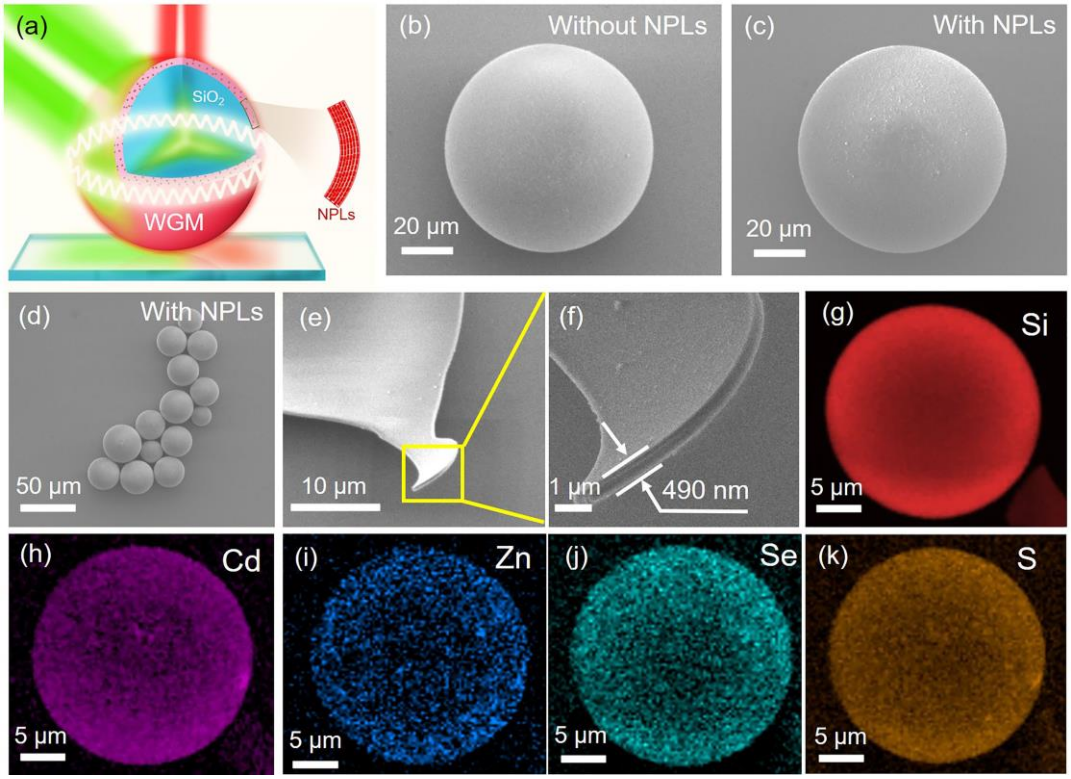

Figure 2. a) Schematic diagram of the NPLs-WGM microsphere in which the CdSe/CdS@$Cd_{1-x}Zn_xS$ Core/Shell NPLs are uniformly covered the whole surface of the microsphere. SEM images of b) bare silica microsphere, c) single NPLs-coated silica microsphere, and d) NPLs-coated microspheres clusters. e) SEM image of the cracker from broken NPLs-coated microsphere. f) Zoom-in image of the cross-section of e). g) EDS elemental mapping results showing the distribution of the chemical elements of NPLs-coated microsphere.

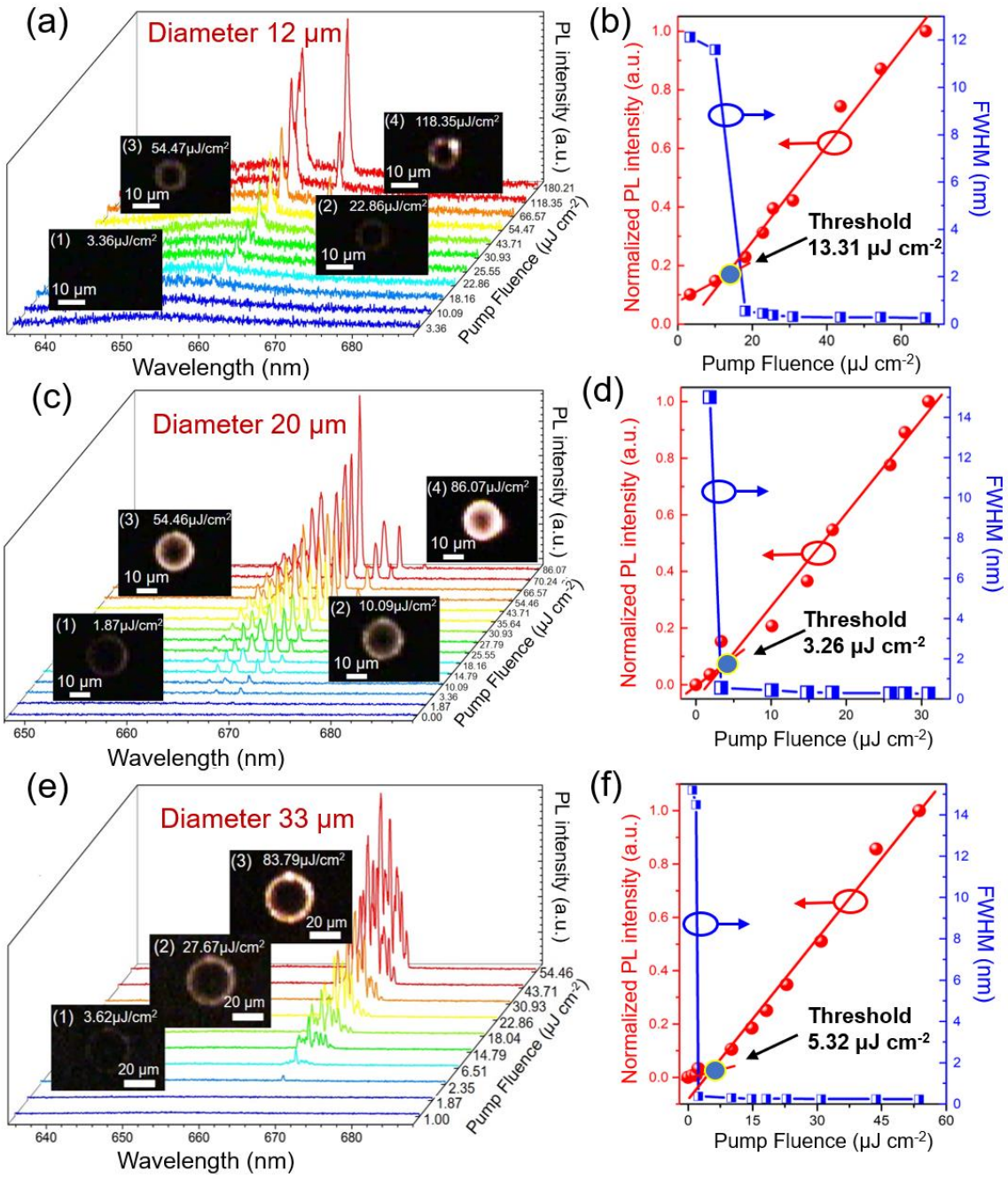

Figure 3. Power-dependent emission spectra of microlasers with different diameters of a) 12 μm, c) 20 μm, and e) 33 μm, respectively. The insets display the microscope photography of the corresponding microlasers under specific excitation power. The clear and bright ring on the surface of the microspheres proves the realization of WGMs lasing. b,d,f) Evolution of the normalized PL intensity and the FWHM of emission peaks as a function of different pump fluence for (a),(c),(e) NPLs-WGM microlasers respectively.

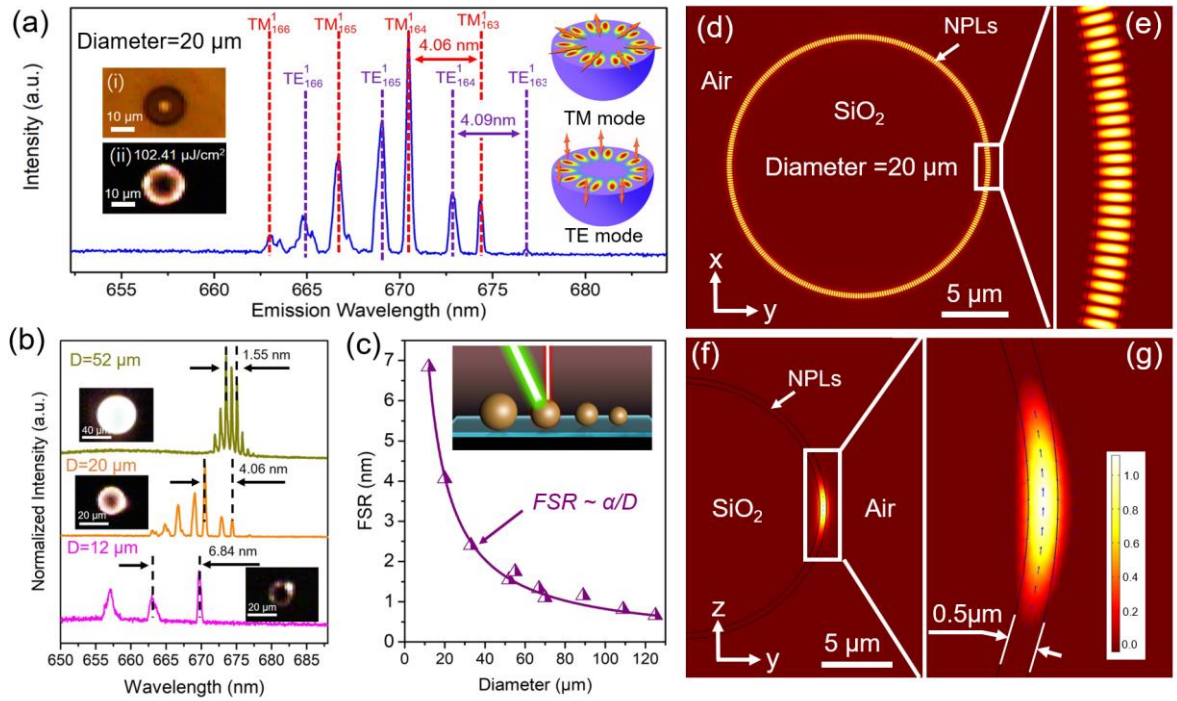

Figure 4. a) Mode analysis of the lasing spectrum from a NPLs-WGM microsphere with a 20 μm diameter. Inset: Schematic views of WGMs with their TE and TM field oscillations. The white arrows represent the orientation of the electric field. b) Lasing spectra from a series of microspheres with a diameter of 12, 20, and 52 μm, respectively. c) The *FSRs* as a function of microsphere's diameter *D*. d) The electric field distributions on the x-y plane. The diameter of the simulated microcavity is 20 μm. e) A magnified view of the electric field profile in d). f) Electric field distributions on the y-z plane. g) A magnified view of the electric field profile in f). For all simulation results, the red and yellow areas represent the lowest and highest field intensities, respectively.

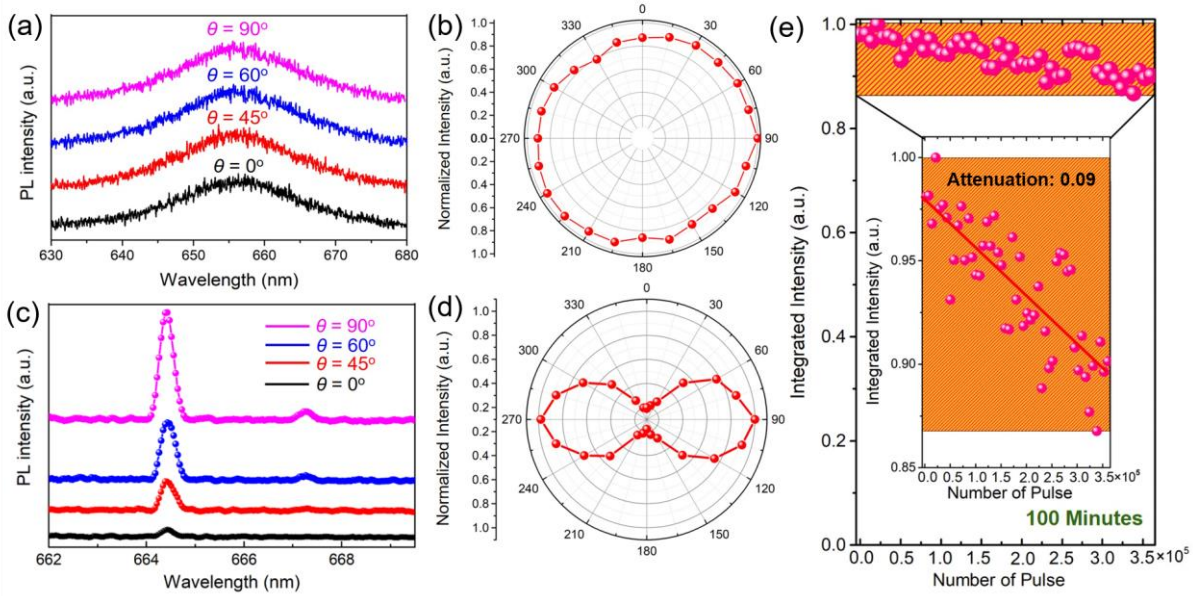

Figure 5. a) Emission spectrum below lasing threshold (~0.76 P_{th}) from a single microlaser under various polarizer rotation angles (θ) of a polarizer. b) The integrated PL intensity as a function of θ. c) Emission spectrum above lasing threshold (~1.72 P_{th}) from the same microlaser recorded under various polarizer rotation angles. d) The integrated lasing peak's intensity as a function of θ. e) Normalized laser intensity under continuously pumped excitation of ~10 times higher than the lasing threshold. To reduce the disturbance caused by the instability of the excitation source, we have performed a linear fit between the relative lasing intensity and the number of pulses.

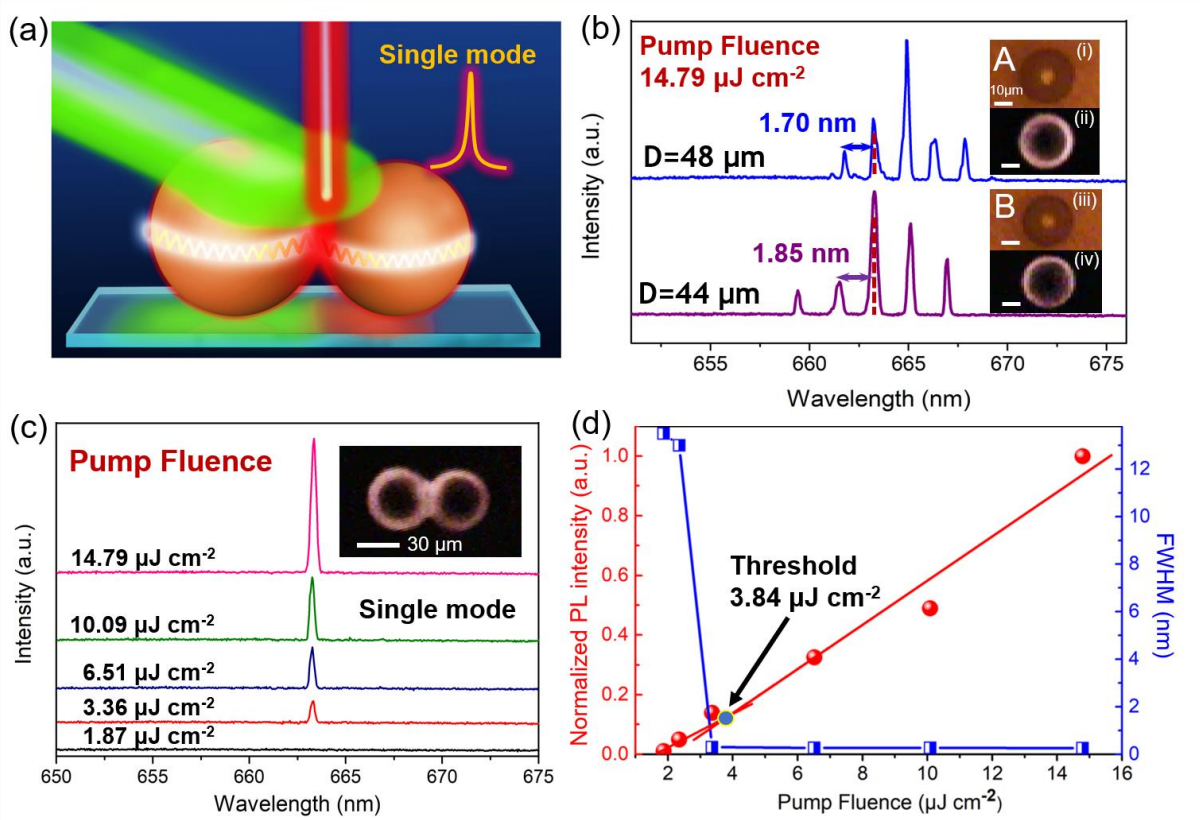

Figure 6. a) Schematic diagram of strong coupling between two NPL-coated microspheres. One microcavity can be regarded as an optical filter of the resonant wavelength of another microcavity to realize a single-mode laser. b) Lasing spectra of isolated microlaser A and microlaser B at a pump fluence of 14.79 μJ cm^{-2}. c) Lasing spectra of a strong coupling system under different pump intensities. PL images of presented microlasers are shown in the insets. (d) The normalized PL intensity and the FWHM of lasing peaks as a function of different pump fluence.

Table of Contents

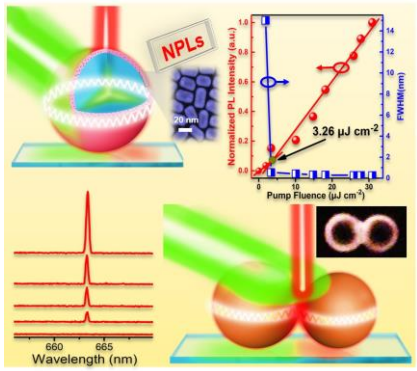

A self-assembled CdSe/CdS@$Cd_{1-x}Zn_xS$ core/shell NPLs-WGM microlaser with ultralow-threshold, tunable-wavelength, and excellent photostability is proposed. Both multi- and single-mode high *Q*-factor WGM lasing are achieved with a record-low lasing threshold of 3.26 μJ cm^{-2}. The results highlight the significance of interface engineering on the optimization of gain properties of heterostructured nanomaterials and shed light on developing future miniaturized tunable coherent light sources.